

Article

Towards Greener Packaging: Tapioca Starch-Based Biocomposites with Siam Weed Extract and Flax Seed Gel as Sustainable Antibacterial Packaging Material

Mohanachandran Nair Sindhu Swapna ^{1,†}, Abin Oscar ^{2,†}, Dorota Korte ¹
and Sankaranarayana Iyer Sankararaman ^{2,*}

¹ Laboratory for Environmental and Life Sciences, University of Nova Gorica, Vipavska 13, SI-5000 Nova Gorica, Slovenia; swapna.nair@ung.si (M.N.S.S.); dorota.korte@ung.si (D.K.)

² Department of Optoelectronics, University of Kerala, Trivandrum 695581, Kerala, India; abin.oscar.peter@gmail.com

* Correspondence: drssraman@gmail.com

† These authors contributed equally to this work.

Abstract: This paper delves into the development of biocomposite (BC) packaging material from tapioca starch (TS), flax seed gel (FS), and Siam weed (SW) extract, considering the increased demand for sustainable, eco-friendly packaging materials. The BCs—BC1 (40 mL), BC2 (80 mL), and BC3 (120 mL), prepared by varying the concentration of SW—were subjected to morphological, structure, thermal, and optical characterisations. The BC with a fragmented, agglomerated morphology shows cellulosic peaks in the X-ray diffraction pattern, indicating the C-type crystalline structure in TS. Thermogravimetric analysis confirmed the BC's safe use up to 300 °C, with a minimal 40% weight loss. Differential scanning calorimetry plots identified heat absorption during gelatinisation, with an endothermic peak at 300 °C marking a phase transition. The Fourier transform infrared (FTIR) and UV–visible spectra revealed functional groups that attribute antibacterial potential to the BC. The optical analyses show greater absorption and fewer emissions, resulting in the increased enthalpy responsible for the microbial activities. Antibacterial studies demonstrated BC2's efficacy against *Staphylococcus aureus*, while the stability against humidity and the minimal weight loss underscored the BC's robust thermal stability. FTIR spectra of post-heating at 80 °C confirmed the structural integrity, positioning the BC as a promising material for eco-friendly packaging solutions.

Keywords: biocomposite; tapioca; flax seed; Siam weed; sustainability



Citation: Swapna, M.N.S.; Oscar, A.; Korte, D.; Sankararaman, S.I. Towards Greener Packaging: Tapioca Starch-Based Biocomposites with Siam Weed Extract and Flax Seed Gel as Sustainable Antibacterial Packaging Material. *Appl. Sci.* **2024**, *14*, 1419. <https://doi.org/10.3390/app14041419>

Academic Editor: Hicham Idriss

Received: 11 January 2024

Revised: 30 January 2024

Accepted: 5 February 2024

Published: 8 February 2024



Copyright: © 2024 by the authors. Licensee MDPI, Basel, Switzerland. This article is an open access article distributed under the terms and conditions of the Creative Commons Attribution (CC BY) license (<https://creativecommons.org/licenses/by/4.0/>).

1. Introduction

The use of plastics is widespread, but it presents significant environmental challenges. The United Nations reports that approximately 11×10^9 kg of plastic waste enters the oceans annually [1,2], forming large plastic pollution patches and endangering marine life. A study published in *Science Advances* reports that the global plastic production has been over 8.3 billion metric tons since the 1950s [3], with only a small portion of it recycled. The remaining plastic waste often ends up in landfills, incinerators, or as litter, taking hundreds of years to decompose. This necessitates the development of biocomposites (BCs) with tailored properties to suit specific applications. Biocomposites, composed of natural-fibre/particle-reinforced polymer matrixes, find diverse applications across various industries [4–6]. In the automotive sector [7], they contribute to the manufacturing of interior components, like door panels and dashboards, as well as exterior elements, such as body panels. The construction industry [8] benefits from biocomposites in structural elements like beams and insulation materials, as they offer eco-friendly alternatives. The versatile applications of biocomposites in consumer goods, the aerospace industry, electronics, and the medical field underscore their potential to create sustainable solutions

across various industries [9]. In the biomedical field, surgical instruments benefit from the combination of strength and biocompatibility that they provide [9]. Ongoing research continues to expand the range of applications for these eco-friendly biocomposite materials.

The packaging industry has witnessed a surge of interest in incorporating sustainable practices, prompted by mounting environmental concerns [5,9]. Bioplastics have gained prominence as a promising solution due to their ability to replace fossil fuel-derived plastics and facilitate a transition towards a more sustainable future. The European Commission's Communication on the EU policy framework classifies bioplastics into compostable, biodegradable, and biobased plastics. Among these, there are biobased bioplastics that are non-degradable [10]. However, there are biodegradable biobased bioplastics that are fetching widespread interest [9,11,12]. Noteworthy are bioplastic options commonly considered in the packaging industry, which include polylactic acid, polyhydroxyalkanoates, polyhydroxybutyrate, polyethylene furanoate, polybutylene succinate, as well as renewable forms of polyethylene and polypropylene [9]. These bioplastics hold immense potential to alleviate environmental pressures and foster a greener trajectory for the packaging sector. One strategy to enhance bioplastics' processing properties and strength involves the incorporation of starch into polyester blends [9,11]. Nevertheless, the available literature [13] indicates that an elevation in the starch content reduces the tensile strength and melt flow index and also causes an increase in the moisture absorption within starch/polybutylene succinate blends. Furthermore, before blending, the starch must undergo a conversion process to become thermoplastic starch, typically involving the use of glycerol. This conversion process extends the production time and associated costs. The glycerol content is also important in the performance of the blends, as a higher glycerol content tends to shift the blends to the brittle side. However, adding glycerol facilitates the process and enhances the crystallinity content [13].

This research paper aims to investigate the use of tapioca starch and Siam weed, two readily available and renewable resources, as integral components in developing bioplastics with enhanced properties. Tapioca starch (TS), derived from the cassava plant, is widely employed in the production of a bioplastic variant known as thermoplastic starch [13]. TS exhibits desirable characteristics, such as renewability and biodegradability, while offering a processing compatibility akin to conventional plastics. Tapioca processing from cassava results in significant amounts of solid waste with high starch and cellulose contents. If left untreated, this waste increases greenhouse gas emissions, exacerbating global climate change [14]. The discarded or unconsumed portions of tapioca, including peels, leftover cooked tapioca, and by-products generated during food preparation, add to the overall waste. Tapioca processing generates liquid and solid waste, accounting for 70–80% of the raw material. Locally known as "onggok", the solid waste produced during the pulping and pressing of cassava constitutes 20–30%, potentially reaching 4–6 million tons of solid waste [14,15]. Thus, the use of tapioca starch in bioplastic manufacturing [16,17] is advantageous due to its abundant availability, cost-effectiveness, and favourable intrinsic properties. Conversely, Siam weed (SW) presents an intriguing composition, comprising 39.6%, 28.7%, 27.5%, and 4.2% cellulose, lignin, hemicellulose, and extractive components, respectively [18]. The significant lignin content in Siam weed renders it a potential substitute for gelatine. Notably, starch and lignocellulosic materials, such as Siam weed, are polysaccharides with comparable chemical structures. From the literature [19,20], it is understood that Siam weed exhibits antimicrobial properties. Consequently, its synergistic interactions within the starch matrix can contribute to the improved performance characteristics of bioplastics with microbial resistance.

This study aimed to develop a biodegradable, biobased, bioplastic packaging material from naturally available tapioca starch, Siam weed extract, and flax seed gel. The work also opens up the possibility of the effective utilization of discarded unconsumed portions of tapioca that balances functionality, environmental responsibility, and the conservation of valuable resources.

2. Materials and Methods

In the present study, the biocomposite films were prepared by using *Manihot esculenta* (or tapioca/cassava starch (TS)) as the base polymer, *Chromolaena odorata* (Siam weed (SW)) as an inhibitor, and flax seed gel (FS) as a binder. The process began by preparing the base polymer, adding 20 g of TS to 200 mL of water, and thoroughly mixing it for 30 min using a magnetic stirrer. The leaves of SW were collected, cleaned, and ground in an agate mortar and pestle using water as the solvent for the preparation of the inhibitor. In this way, 500 mL of leaf extract was prepared from 100 g of leaves. Next, the leaf extract was added to the starch solution in three different concentrations, 40 mL, 80 mL, and 120 mL, and stirred for 30 min. To this mixture containing the TS and SW, binder FS was added and stirred for 1 h till a slurry solution was obtained. Then, it was poured into a mould to form sheets and allowed to sun dry for 24 h, followed by an air-drying period of 24 h, forming thin sheets of biocomposite material. The biocomposite samples with 40 mL, 80 mL, and 120 mL SW extracts, labelled as BC1, BC2, and BC3, respectively, were subjected to various characterisations to find their applications in day-to-day life and industries.

The investigation of the biocomposites involved a thorough exploration of their physical, optical, and antibacterial properties. The samples' morphologies and structures are understood from the field-emission scanning electron microscopic (FESEM—Nova Nano, FEI, Hillsboro, OR, USA) images and X-ray diffraction (Bruker D8 ADVANCE—XRD, Billerica, MA, USA) patterns. The composites' thermal stabilities and yields were studied through thermogravimetric analysis (TGA) employing the PerkinElmer (Waltham, MA, USA) simultaneous thermal analyser 6000, and vibrational mode analysis within the 4000–400 cm^{-1} range was conducted using a PerkinElmer Fourier Transform Infrared (FTIR) spectrometer. The composites' optical characteristics, like the absorption and optical emissions, were obtained through the Jasco (Oklahoma City, OK, USA) V550 Ultraviolet-visible (UV-Vis) absorption spectrometer and the Horiba (Kyoto City, Japan) Fluorolog TCSPC photoluminescence spectrometer, respectively. The antibacterial properties of all the biocomposites were identified using the agar-well diffusion method. The goal of this multifaceted analysis was to offer a thorough comprehension of the varied properties displayed by the composite material.

3. Results and Discussion

A biocomposite's morphology is crucial for specific applications, like biopackaging, biomedicine, and electronics, where the effective surface area plays a crucial role. An FESEM image of starch and the biocomposite BC1 as a representative (as BC2 and BC3 also exhibit the same morphology) is shown in Figure 1. When the starch shows stacked laminae, BC1 shows fragmented, agglomerated structures. The crystalline characteristics and amorphous structures of the cellulose-based materials are understood from the sharp and broad XRD peaks. Starch displays various polymorphs that are distinguished by unique crystalline structures. The primary polymorphs include A-type, B-type, and C-type starches, each characterised by a distinct arrangement of starch molecules within its crystalline lattice [21,22]. Starch with a C-type crystalline structure, derived from legumes or plant roots like pea seeds or cassava roots, features a unique composition formed by the coexistence of A- and B-type crystallites [21,22]. Specifically, C-type starch has a B-type structured core surrounded by A-type crystallites. The base polymer's (TS) XRD pattern shown in Figure 2a exhibits peaks at 15° , 17.97° , 19.93° , 22.78° , 28.7° , 30.69° , and 40.21° that correspond to the C-type crystallite structure of TS. The XRD pattern of the representative biocomposite, BC1, shown in Figure 2b, also exhibits peaks at 17.83° (-102), 19.6° (021), 20.4° (002), 21.6° (012), 28° (210), and 32.03° (013), which are assigned to the cellulosic peaks in comparison with the ICDD data (00-003-0226) indicating the C-type crystalline structure in TS.

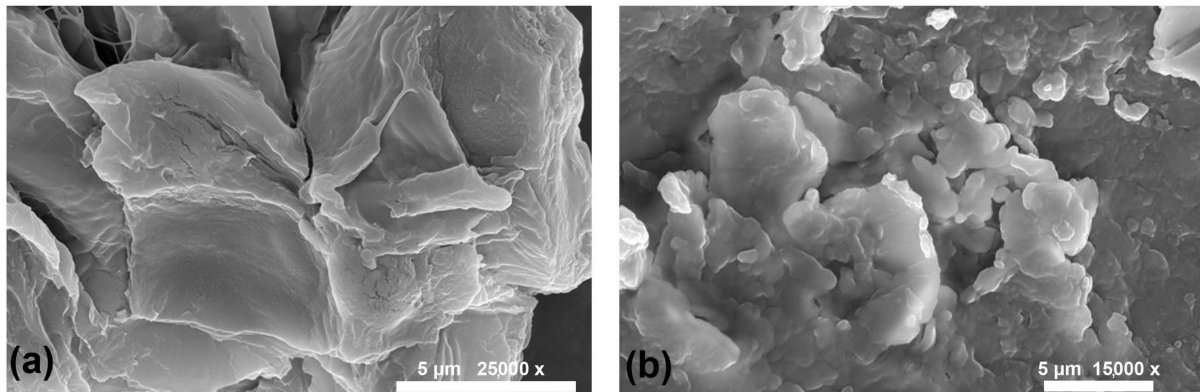


Figure 1. FESEM of (a) TS (b) BC1.

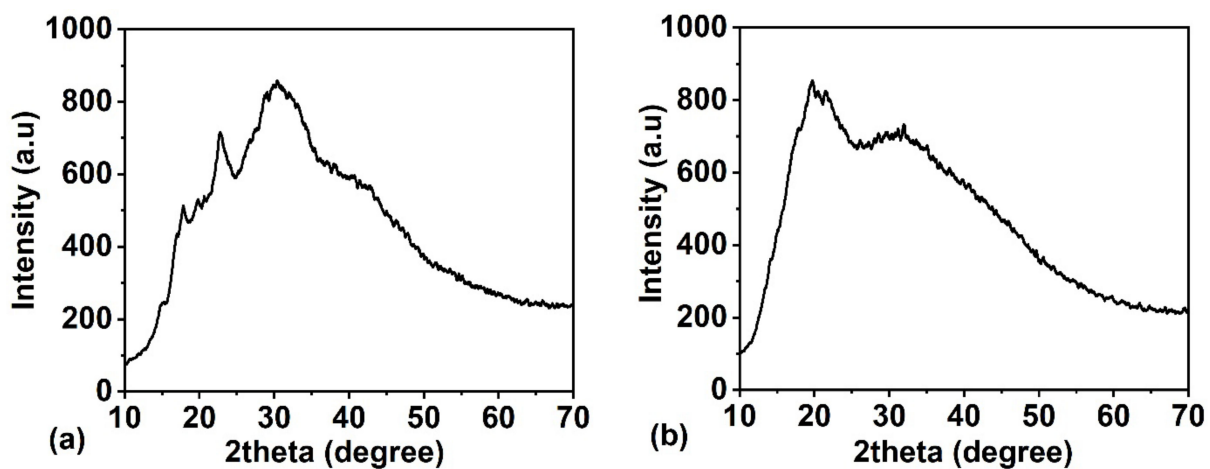


Figure 2. XRD patterns of (a) TS and (b) BC1.

The thermal stability of biocomposite materials is a critical factor that can positively impact their performance, durability, and suitability for diverse applications, spanning from construction and automotive applications to electronics and beyond. The literature [23,24] indicates that starch undergoes a small initial weight loss up to 100 °C as a result of moisture removal. Subsequently, between 100 and 200 °C, the weight loss occurs as a result of the elimination of absorbed water resulting from gelatinisation. The highest decomposition occurs around 200–400 °C, and it is attributed to the breaking of glycosidic bonds in the starch. The TG and DTG analysis plots of the biocomposite BC1 are displayed in Figure 3a and b, respectively. The TGA curve exhibits three stages of thermal decomposition that occurred in the sample: up to 250 °C; between 250 °C and 340 °C; and from 340 °C to 800 °C. A weight reduction of 11.40% in the initial stage, up to 250 °C, can be attributed to the evaporation of water adsorbed on the surface of the composite and the removal of amorphous carbon. Between 250 °C and 340 °C, the composite experienced its most significant weight loss, amounting to 51.96%. This points to the peak decomposition of the composite, likely due to the oxidation of the partially decomposed starch and the fibre degradation. After 340 °C, the TGA curve shows a plateau region, as the remaining residue was typically composed of inorganic ash. The ash content represents the incomplete combustion of the organic components of the starch [24]. From the DTG analysis (Figure 3b), 300 °C can be considered as the safe limit for using the prepared biocomposite, where the TGA curve shows only a 40% weight loss.

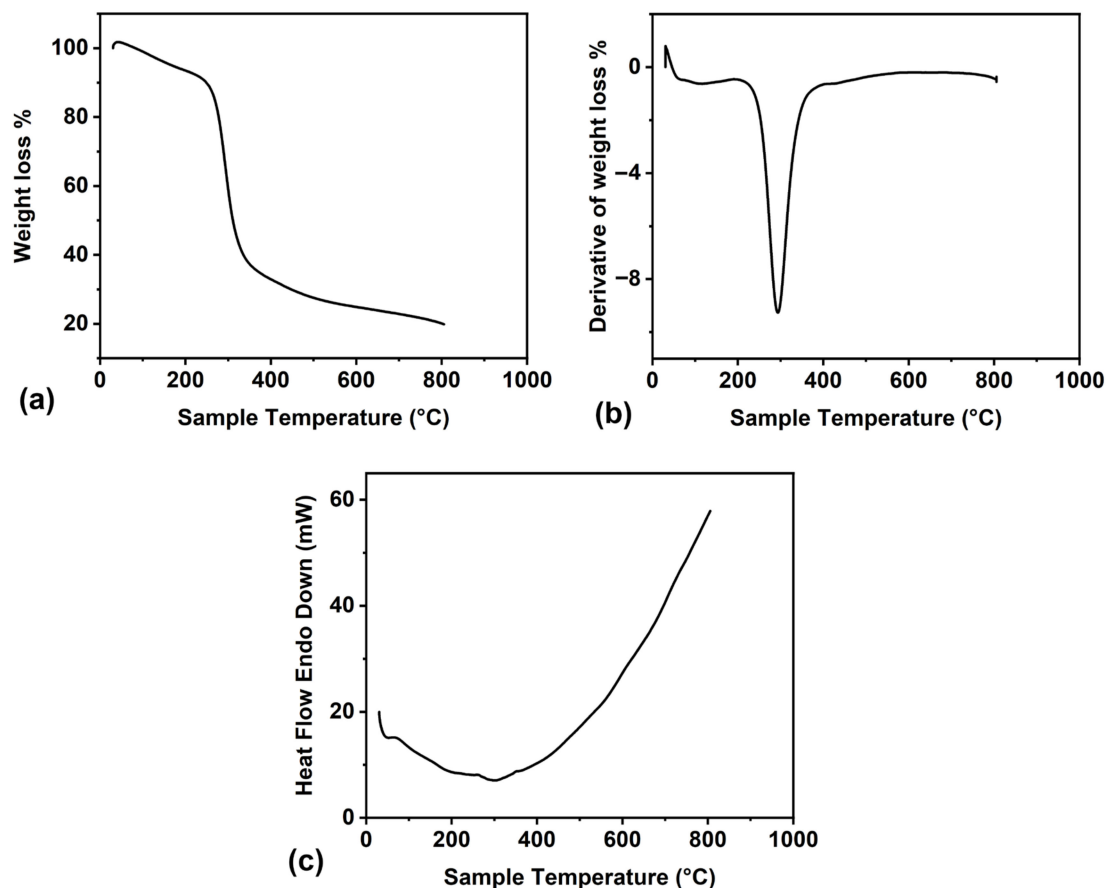


Figure 3. (a) TGA, (b) DTGA, and (c) DSC of BC1.

DSC is a thermal analysis method employed for examining the heat flow linked to the physical and chemical transitions within a sample observed in relation to temperature variations. This information helps characterise various properties, such as the phase transitions, melting points, and heat capacity, providing valuable insights into the material's thermal behaviour and stability. According to the literature, TS typically exhibits endothermic peaks in the DSC thermogram, corresponding to events such as gelatinisation and retrogradation [23]. The DSC plot of the biocomposite BC1, shown in Figure 3c, exhibits endothermic peaks at 50 °C and 300 °C. The peak at 50 °C observed in the DSC plot of TS corresponds to the gelatinisation process. Tapioca starch, composed of amylose and amylopectin molecules in granules, undergoes gelatinisation when exposed to heat and water. This complex thermodynamic transition involves heat absorption, disrupting hydrogen bonds, allowing water penetration, and resulting in the swelling and hydration of the starch granules. The endothermic peak in the DSC plot signifies the heat absorption required for gelatinisation, and its temperature indicates the onset of this process. The endothermic peak at 300 °C indicates the phase transition of the composite by evaporation or sublimation due to the decomposition of the sample and removal of amorphous carbon [23]. Thus, thermal analysis provides insights into the composite's thermal behaviour, aiding in understanding its functional properties for bioplastic packaging applications.

FTIR spectroscopy is a versatile analytical technique with several advantages in analysing biocomposites. It enables comprehensive chemical composition analysis, identifying individual components and their respective functional groups. The FTIR spectra of the biocomposites BC1, BC2, and BC3 are shown in Figure 4, with their peak assignments in Table 1. The proteins often contain amide bonds, and the N-H stretching and bending vibrations typically appear in the regions around 3300 cm^{-1} and 1600–1500 cm^{-1} , the O-H stretching vibrations appear around 3300 cm^{-1} , the carbonyl stretching vibrations appear around 1700–1750 cm^{-1} , the C=C stretching vibrations appear around 1600–1500 cm^{-1} ,

and P=O stretching appears around 1000–1300 cm^{-1} [13,23,25–29]. These functional groups indicate the possibility of the presence of various antibacterial compounds in the sample.

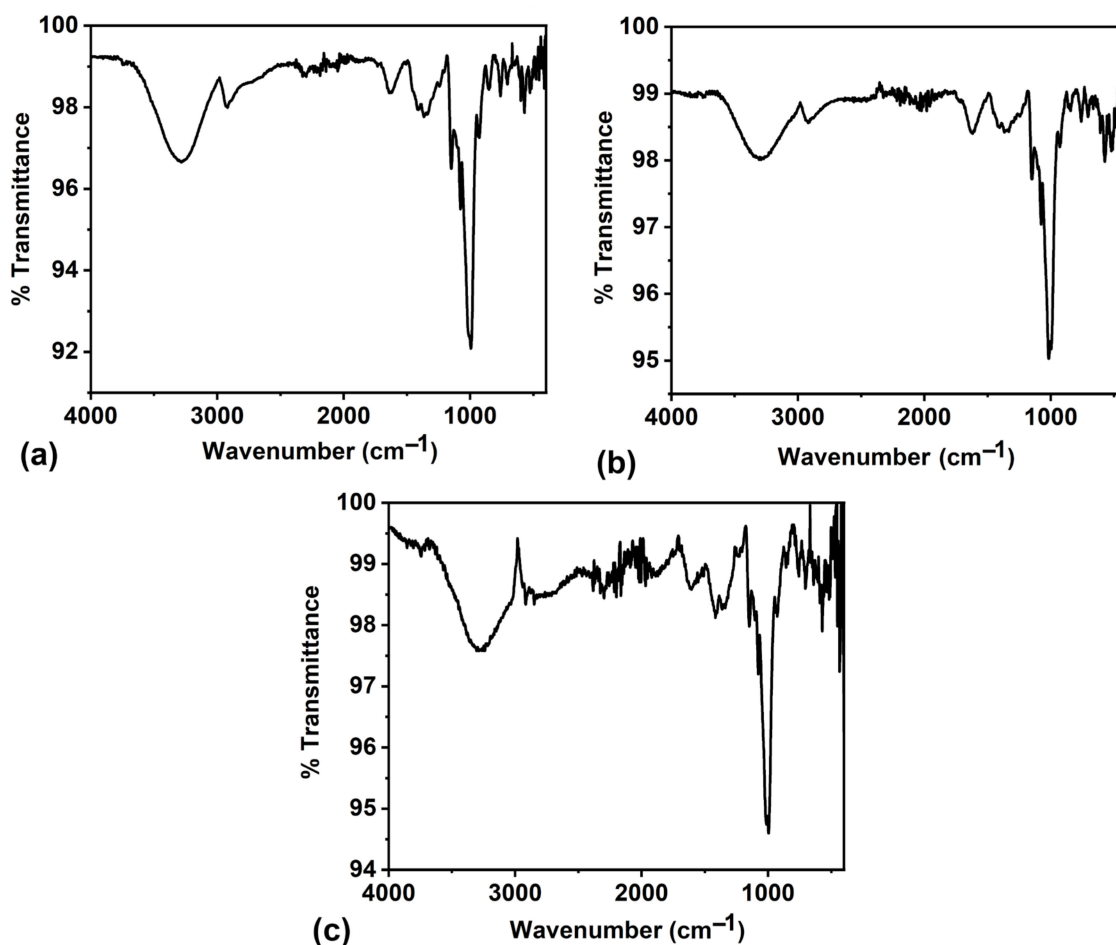


Figure 4. FTIR spectrum of (a) BC1, (b) BC2, and (c) BC3.

Table 1. FTIR peak assignments.

	Samples			Functional Groups with References
	BC1	BC2	BC3	
	3283	3291	3266	O-H stretching vibration [23] and N-H stretching secondary amines [25]
	2918	2919	2916	
	-	-	2850	CH ₂ asymmetric stretching of glucose rings [23]
	2307	-	-	CH ₂ symmetric stretching
	1728	-	1748	O=C=O stretching
	1628	1620	1614	C=O stretching [26]
	1417	1425	1417	C=C stretching, O-H bending, or Amide I vibrations [27]
	1366	1367	1362	CH ₂ bending [28]
	1339	1343	1339	C-H symmetric bending [28]
	1149	1148	1148	Methylene C-H bending [28]
	1077	1069	1080	C-C and C-O stretching [26]
	<1000	<1000	<1000	P=O stretching of proteins [27]
Wavenumber (cm^{-1})				C-O-C stretching vibrations and C-O-H bending vibrations in amylose and amylopectin [13,29]

The UV spectral study of bioplastic packaging materials provides valuable insights into their molecular compositions and structural characteristics and is particularly useful for analysing the electronic transitions of organic compounds. The broad UV-visible spectrum suggests the presence of a chromophore that absorbs in the UV-visible range. The UV-visible absorption spectrum of the composites are displayed in Figure 5. They show a broad absorption peak at 360 nm and small humps at 213 nm and 656 nm. The occurrence

of a broad peak in the UV–visible spectrum is due to the presence of conjugated systems or electronic transitions within the molecules. Conjugated systems, which consist of alternating single and double bonds or aromatic structures, are responsible for the absorption in the UV region. The broader the peak, the more complex the conjugated system or the greater the number of electronic transitions involved. The factors contributing to the broadening of peaks in the UV spectrum are longer conjugation lengths, π - π^* electronic transitions, and the molecular structure. Siam weed contributed to the peak at 656 nm, indicating chlorophyll in the biocomposite. From Figure 5d, it can be observed that adding more Siam weed extract does not significantly affect the optical absorption (i.e., the absorbance level increases from sample BC1 to BC2 and, further, there is no significant change in BC3). The Tauc plot analysis of Figure 5a–c yields direct bandgap energies of 2.08 eV, 2.14 eV, and 2.05 eV for the BC1, BC2, and BC3 samples, respectively.

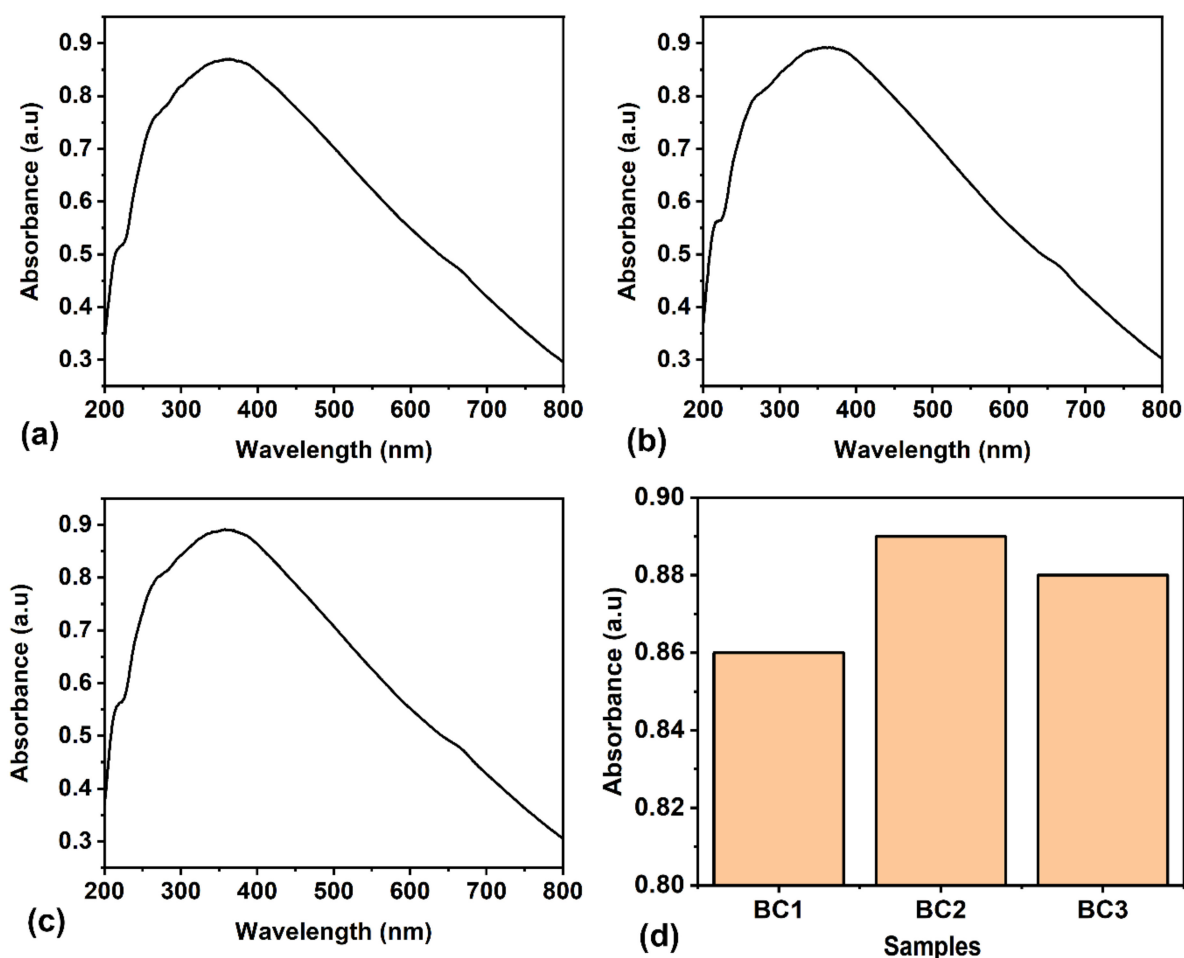


Figure 5. UV–visible absorption spectrum of samples: (a) BC1, (b) BC2, and (c) BC3; (d) absorbance at 360 nm for all three samples.

Photoluminescence (PL) spectral studies of biopackaging materials provide valuable information about their optical and photophysical characteristics. The emission peaks and intensity in the PL spectrum can indicate the material's composition and molecular arrangement and the presence of specific fluorophores or chromophores. By studying the PL properties of bioplastic packaging materials, researchers can gain insights into their fluorescence behaviour, which is crucial for product labelling or tracking applications. The PL spectra of BC1, BC2, and BC3 for the excitations 300 nm, 350 nm, 400 nm, and 450 nm are shown in Figure 6. All the samples exhibited broad emissions at 425 nm irrespective of the excitation. The addition of Siam weed lowered the emission intensity (i.e., the emissions decrease from the BC1 sample to the BC2 sample and, further, there is

no significant change in BC3). A representative variation in the emission intensity peak at 440 nm corresponding to the excitation at 350 nm is shown in Figure 6e. When the PL spectrum is analysed in light of Figure 5, it is observed that although the absorbance level increases from BC1 to BC2, the emission behaviour is just the opposite. The optical energy distribution in the emission spectrum can be understood from the power spectral analysis and the colour purities of the emissions from the CIE plot. The representative power spectrum and CIE plot corresponding to the 350 nm excitation are shown in Figures 7 and 8, respectively. The samples BC1, BC2, and BC3 exhibited emissions in the blue region with colour purities of 38.5%, 48.5%, and 50.1%, respectively. From the PL analyses, it can be inferred that more energy was dissipated by non-radiative deexcitation, raising the system enthalpy. The change in enthalpy can help with the biological activity of the sample, which is understood from the antimicrobial studies.

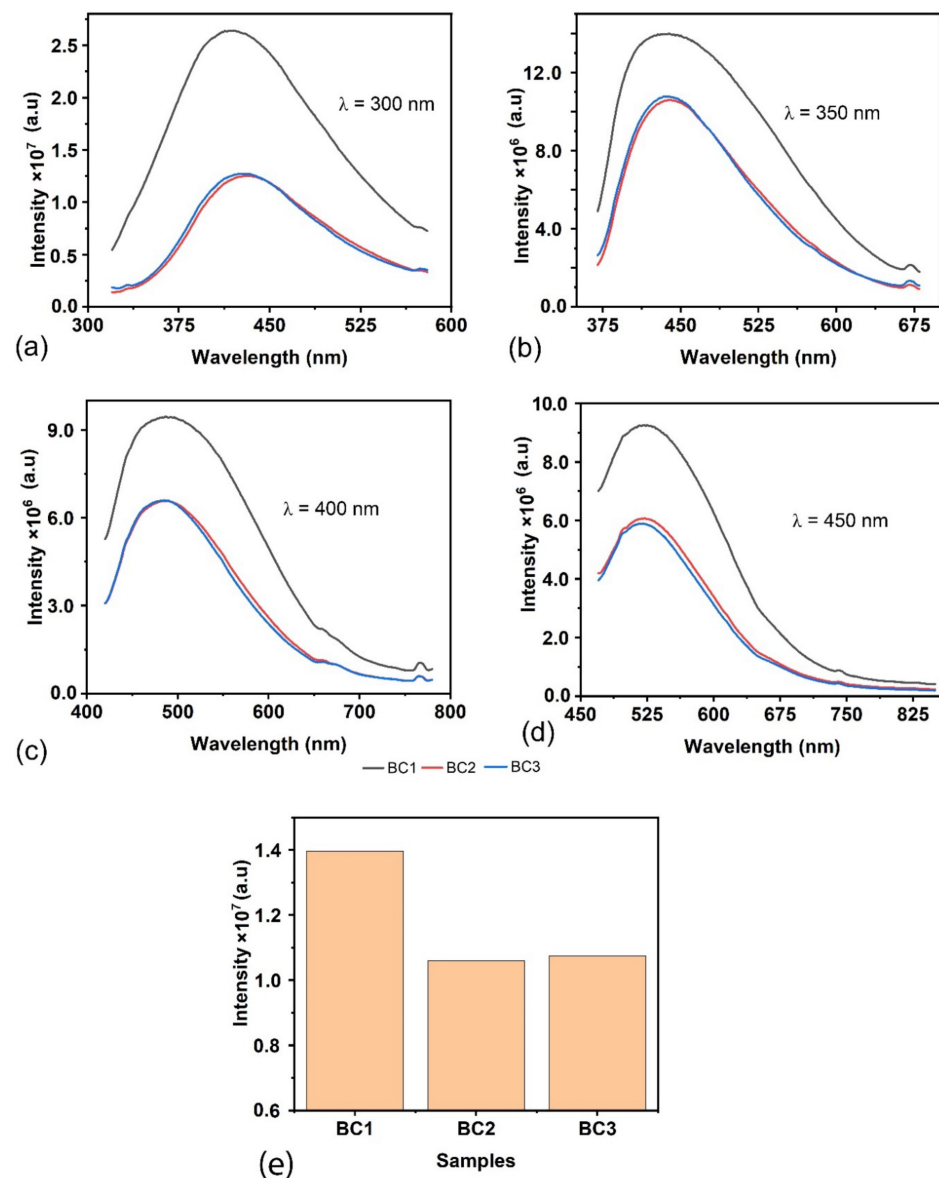


Figure 6. PL spectra of samples for the wavelengths (λ) of excitations at (a) 300 nm, (b) 350 nm, (c) 400 nm, and (d) 450 nm; (e) variation in emission intensity peaks at 440 nm corresponding to the excitation at 350 nm.

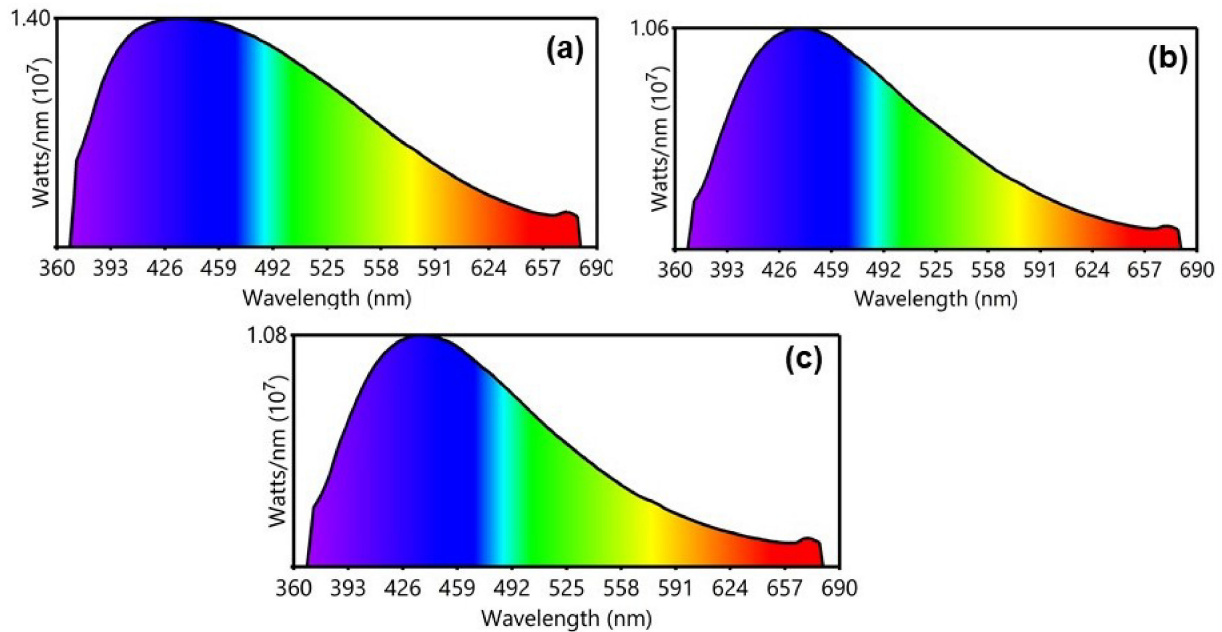


Figure 7. Power spectra of samples: (a) BC1, (b) BC2, and (c) BC3 for wavelengths (λ) of excitation at 350 nm.

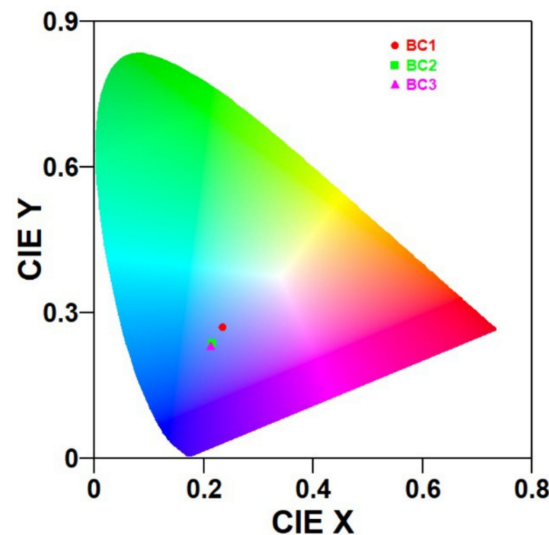


Figure 8. CIE plot of samples: BC1, BC2, and BC3 for wavelengths (λ) of excitation at 350 nm.

Antibacterial analysis helps determine the biocomposite's potential to inhibit or reduce the growth of bacteria, providing valuable information for applications in fields such as medical devices and food packaging. In the present study, the antibacterial properties of the biocomposites against the Gram-negative *Staphylococcus aureus* and Gram-positive *Pseudomonas aeruginosa* were investigated. It is well known that *Pseudomonas aeruginosa* [30–32] causes severe infections in immunocompromised individuals, leading to conditions such as pneumonia, urinary tract infections, and bloodstream infections, and *Staphylococcus aureus* [31,33] causes infections like streptococcal infections (e.g., strep throat, scarlet fever), Clostridium difficile infections, listeriosis, enterococcal infections, diphtheria, anthrax, and tetanus. Both bacteria are capable of forming biofilms, which are slimy layers of microorganisms embedded in an extracellular matrix. Biofilms on packaging materials can create an environment for other microorganisms to thrive, leading to the deterioration of the material and potentially affecting the integrity of the packaging [34].

The agar-well diffusion method was employed to assess the samples' antibacterial efficacies against both Gram-positive (*Pseudomonas aeruginosa*) and Gram-negative (*Staphylococcus aureus*) bacteria. Petri plates, each having 20 mL of Muller Hinton Agar

Medium, were inoculated with cultures of Gram-negative and Gram-positive bacteria. The bacterial cultures were adjusted based on the McFarland Standard. Wells, approximately 10 mm in diameter, were created using a well cutter, and two different concentrations of the sample (1 $\mu\text{g}/\mu\text{L}$ and 4 $\mu\text{g}/\mu\text{L}$) were introduced into two different wells. Subsequently, the Petri plates were incubated at 37 °C for 24 h. During this incubation period, the antimicrobial components from the samples diffuse into the medium and interact with the freshly seeded test organisms on the plates. The standard antibacterial agent streptomycin served as the positive control in this experiment. The resulting zones of inhibition exhibited a uniform circular pattern due to the confluent lawn of bacterial growth. The antibacterial activity was quantified by measuring the inhibition zone's diameter surrounding each well, representing the bacterial resistance to the antimicrobial agent. A larger zone generally indicates greater susceptibility, while a smaller or absent zone may suggest resistance. The interpretation of the results was based on established guidelines and breakpoints provided by the European Committee on Antimicrobial Susceptibility Testing. The zones of inhibition against *Staphylococcus aureus* and *Pseudomonas aeruginosa* are displayed in Figure 9a and 9b respectively, and the zone diameters are shown in Table 2. The higher concentration of BC2 shows the highest zone diameter, followed by the higher concentration of BC1. The packaging developed using this biocomposite is resistant to *Staphylococcus aureus* infections. The negative results observed for all samples against Gram-negative bacteria could be attributed to their more intricate cell wall structure than that of Gram-positive bacteria. Their cell walls consist of a thin peptidoglycan layer surrounded by an outer membrane. This outer membrane contains lipopolysaccharides, which are important for the pathogenicity of many Gram-negative bacteria. This is why Gram-negative bacteria exhibit greater resistance than Gram-positive bacteria [35]. From the literature [36,37], it can be seen that the FTIR spectra of materials exhibiting antibacterial properties show peaks corresponding to the N-H, C=O, and C=C, vibrational modes. The antibacterial properties exhibited by the biocomposites can be attributed to the presence of these bonds observed in the FTIR spectra shown in Figure 4.

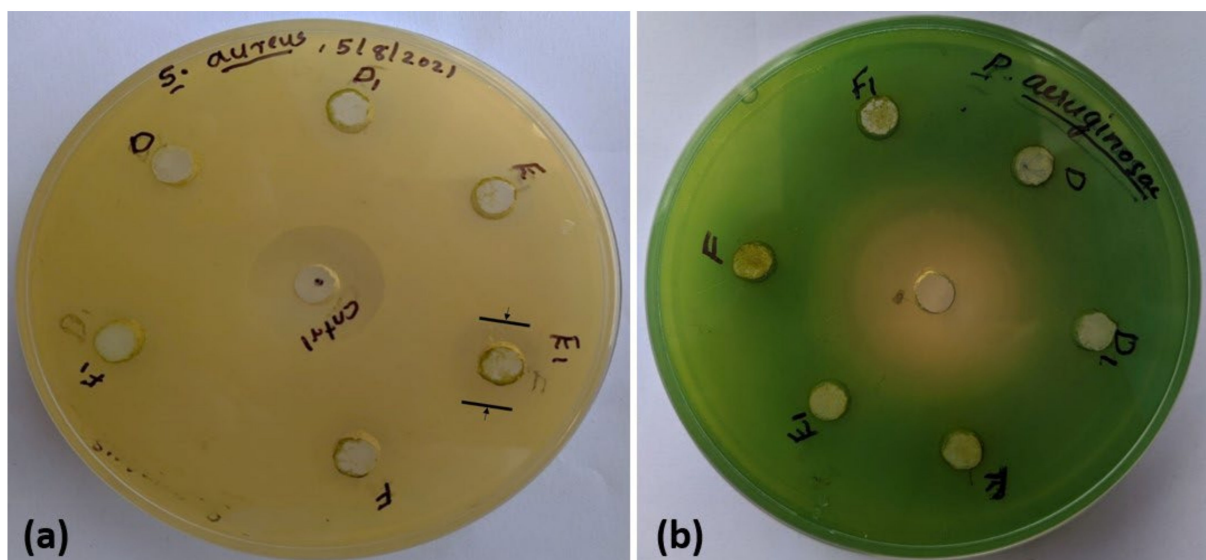


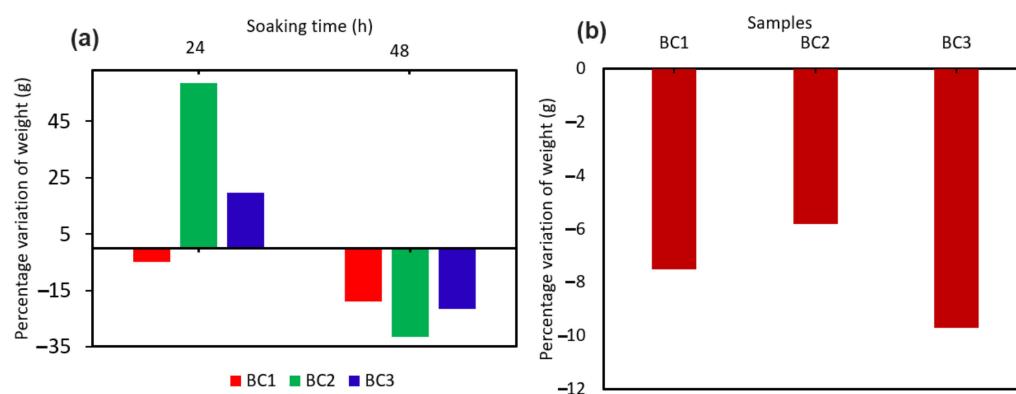
Figure 9. Antibacterial analysis of the samples showing the zones of inhibition against (a) *Staphylococcus aureus* and (b) *Pseudomonas aeruginosa*. (D—BC1, 1 $\mu\text{g}/\mu\text{L}$; D1—BC1, 4 $\mu\text{g}/\mu\text{L}$; E—BC2, 1 $\mu\text{g}/\mu\text{L}$; E1—BC2, 4 $\mu\text{g}/\mu\text{L}$; F—BC3, 1 $\mu\text{g}/\mu\text{L}$; F1—BC1, 4 $\mu\text{g}/\mu\text{L}$).

Table 2. Zone diameters of samples against Gram-positive and Gram-negative bacteria.

	Sample		Radius (mm)
<i>Staphylococcus aureus</i> (Gram-positive)	Control	Streptomycin	2.1
	BC1	4 µg/µL	1.2
		1 µg/µL	0.8
	BC2	4 µg/µL	1.5
		1 µg/µL	1.1
	BC3	4 µg/µL	1.0
1 µg/µL		1.0	
<i>Pseudomonas aeruginosa</i> (Gram-negative)	BC1	4 µg/µL and 1 µg/µL	No zone
	BC2		
	BC3		

The antibacterial action in a biocomposite containing TS, FS, and SW results from the combined effects of their individual antimicrobial properties. Tapioca starch, acting as a matrix, facilitates the dispersion and release of antimicrobial agents from the other components. Flax seed gel contributes bioactive compounds [38], such as polyphenols and lignans, which can disrupt bacterial cell walls and membranes. With its flavonoids, alkaloids, and tannins, Siam weed extract [19] further enhances the antibacterial activity by potentially interfering with bacterial enzymes and DNA replication. The synergistic effects of these components, along with the physical properties of the biocomposite, create a formulation that may effectively inhibit bacterial growth and provide a promising avenue for antibacterial applications.

The water solubilities of the samples were studied by immersing them in water for 24 h and 48 h, and the process was repeated seven times. The percentage variation in the weights for the biocomposites is shown in Figure 10a. The water solubility study of biocomposites holds significant importance due to its implications across various fields. This analysis is crucial for assessing the environmental impact and biodegradability of biocomposites and provides insights into their behaviour in moist or wet conditions. The study helps understand bioactive compounds' release kinetics, influencing applications in drug delivery, agriculture, and food packaging. Additionally, it serves as a quality control measure during manufacturing, ensuring consistent properties and reliability. In biomedical and agricultural applications, knowledge of the water solubility of a material is vital for evaluating its safety and predicting its lifespan in specific environments. Figure 10a shows that the BC2 and BC3 samples remained insoluble for up to 24 h, indicated by the positive percentage variation in their weights. However, all three samples showed weight loss after 48 h of immersion in water. It is worth noting that the maximum weight loss percentage was only 31.4% after 48 h of immersion in water. Hence, the samples can exhibit good stability against atmospheric humidity variation when they are used for packaging.

**Figure 10.** Percentage variation in weights of biocomposites (a) after soaking for 24 h and 48 h and (b) heated at 80 °C for 2 h after soaking for 48 h.

The temperature study of biocomposites is pivotal for optimising manufacturing processes, assessing the thermal stability, and predicting the material performance. Understanding how biocomposites respond to temperature variations is crucial for ensuring the integrity of their structures and functional properties during processing and potential exposure to different environments. This knowledge informs the selection of appropriate materials for specific applications. Temperature studies enhance biocomposites' overall reliability, durability, and efficiency. The samples, soaked for 48 h in water, were heated at 80 °C for 2 h in an air oven, and the percentage variation in the weights for the samples is shown in Figure 10b. The study reveals that the weight loss was minimal (5.8%) for sample BC2, and the maximum weight loss obtained was only 9.8% for sample BC3. The study points to the thermal stability of the composites. To confirm that the biocomposites did not undergo any structure modifications, the FTIR spectra of the samples heated at 80 °C were recorded and are shown in Figure 11. The spectra show no structure modifications, confirming the stability and suitability of the biocomposites for biopackaging.

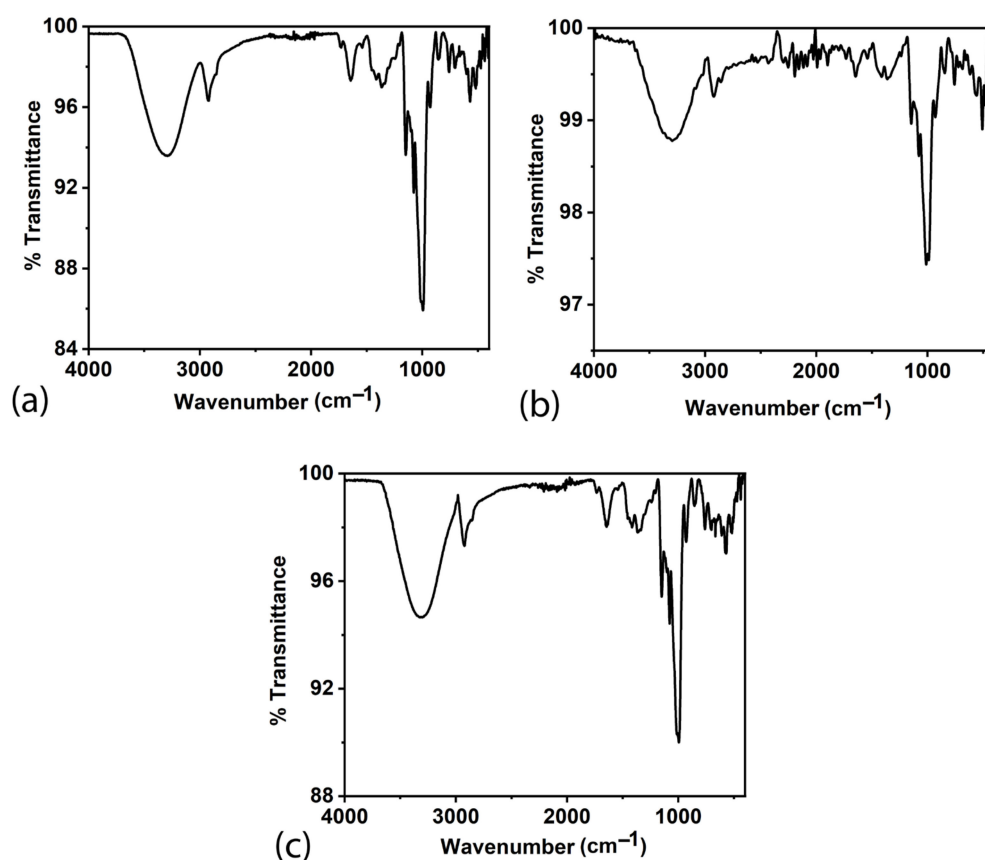


Figure 11. FTIR spectra of samples heated at 80 °C: (a) BC1, (b) BC2, and (c) BC3.

4. Conclusions

Investigations on sustainable packaging materials are highly significant because they play a crucial role in lessening the burden on landfills and ecosystems. The analysis of the structures and thermal properties of biocomposite materials provides information about the quality of the packaging materials developed. This study presents the development and comprehensive characterisation of biocomposites derived from TS, FS, and SW, with varying concentrations of SW extract. The FESEM images revealed fragmented, agglomerated structures in BC1, contrasting with the stacked laminae observed in starch. The XRD pattern exhibited cellulosic peaks corresponding to the C-type crystalline structure in TS. TG analysis established the biocomposite's safe usage up to 300 °C, supported by a minimal 40% weight loss in the TGA curve. The DSC plot indicated heat absorption during gelatinisation, with an endothermic peak at 300 °C marking the composite's phase

transition. The functional groups (-N-H stretching, bending, carbonyl stretching, C=C stretching vibrations, P=O stretching) in the sample are identified from the FTIR spectrum, suggesting its potential as an antibacterial compound. The UV-visible spectrum shows a broad absorption peak at 360 nm and smaller humps at 213 nm and 656 nm, indicating conjugated systems or electronic transitions and chlorophyll. The absorbance analysis also revealed the insensitivity of optical absorption to additional SW extract. In the PL spectrum analysis, the emission behaviour was the opposite, while the absorbance levels increased from BC1 to BC2. Power spectral analysis and the colour purity from the CIE plot explain the emission spectrum's optical energy distribution, revealing emissions in the blue region with nearly 50% colour purity. Increased energy dissipation through non-radiative deexcitation impacts the system's enthalpy, potentially influencing the biological activity. The antibacterial studies demonstrated the heightened effectiveness of BC2, with the increased BC1 concentration also showing efficacy, particularly in resisting *Staphylococcus aureus* infections. Despite the limited impact on Gram-negative bacteria, the biocomposite exhibited commendable stability against atmospheric humidity variations, which is a critical characteristic for biopackaging. Temperature studies underscored minimal weight loss, highlighting the composite's robust thermal stability. FTIR spectra of post-heating at 80 °C confirmed the structural integrity, affirming the biocomposite's suitability for bioplastic packaging applications. These findings position the discarded unconsumed portions of tapioca as a promising and stable material for eco-friendly packaging solutions.

Author Contributions: Methodology, M.N.S.S. and A.O.; Validation, D.K.; Formal analysis, M.N.S.S., A.O. and S.I.S.; Investigation, M.N.S.S. and D.K.; Resources, A.O.; Writing—original draft, M.N.S.S. and S.I.S.; Writing—review & editing, D.K. and S.I.S.; Visualization, S.I.S.; Supervision, S.I.S. All authors have read and agreed to the published version of the manuscript.

Funding: The authors Mohanachandran Nair Sindhu Swapna and Dorota Korte acknowledge the financial support from the Slovenian Research Agency (project (No. J7-2602) and program (No. P2-0393).

Institutional Review Board Statement: Not applicable.

Informed Consent Statement: Not applicable.

Data Availability Statement: The data that support the finding of this study are available from the corresponding author upon reasonable request.

Conflicts of Interest: The authors declare no conflicts of interest.

References

1. Madaan, S. What Is Plastic Pollution? 2018, pp. 1–6. Available online: <https://www.earthclipse.com/environment/environmental-effects-plastic-pollution.html> (accessed on 20 March 2023).
2. United Nations. Sustainable Development Goals. 2023. Available online: <https://www.un.org/sustainabledevelopment/sustainable-development-goals/> (accessed on 20 March 2023).
3. Geyer, R.; Jambeck, J.R.; Law, K.L. Production, use, and fate of all plastics ever made. *Sci. Adv.* **2017**, *3*, e1700782. [CrossRef]
4. Bushra, A.; Subhani, A.; Islam, N. A comprehensive review on biological and environmental applications of chitosan-hydroxyapatite biocomposites. *Compos. Part C Open Access* **2023**, *12*, 100402. [CrossRef]
5. Chueangchayaphan, W.; Nooun, P.; Ummarat, N.; Chueangchayaphan, N. Eco-friendly biocomposite foam from natural rubber latex and rice starch for sustainable packaging applications. *Express Polym. Lett.* **2024**, *18*, 27–40. [CrossRef]
6. Phiri, R.; Mavinkere Rangappa, S.; Siengchin, S.; Oladijo, O.P.; Dhakal, H.N. Development of sustainable biopolymer-based composites for lightweight applications from agricultural waste biomass: A review. *Adv. Ind. Eng. Polym. Res.* **2023**, *6*, 436–450. [CrossRef]
7. Alam, M.A.; Sapuan, S.M.; Ya, H.H.; Hussain, P.B.; Azeem, M.; Ilyas, R.A. Application of biocomposites in automotive components: A review. In *Biocomposite and Synthetic Composites for Automotive Applications*; Elsevier: Amsterdam, The Netherlands, 2021; pp. 1–17. [CrossRef]
8. Ryłko-Polak, I.; Komala, W.; Białowiec, A. The Reuse of Biomass and Industrial Waste in Biocomposite Construction Materials for Decreasing Natural Resource Use and Mitigating the Environmental Impact of the Construction Industry: A Review. *Materials* **2022**, *15*, 4078. [CrossRef]
9. Pilla, S. Engineering applications of bioplastics and biocomposites—An overview. In *Handbook of Bioplastics and Biocomposites Engineering Applications*; John Wiley & Sons, Inc.: Hoboken, NJ, USA, 2011; pp. 1–15. ISBN 9780470626078.

10. Briassoulis, D.; Pikasi, A.; Hiskakis, M. End-of-waste life: Inventory of alternative end-of-use recirculation routes of bio-based plastics in the European Union context. *Crit. Rev. Environ. Sci. Technol.* **2019**, *49*, 1835–1892. [[CrossRef](#)]
11. Jayarathna, S.; Andersson, M.; Andersson, R. Recent Advances in Starch-Based Blends and Composites for Bioplastics Applications. *Polymers* **2022**, *14*, 4557. [[CrossRef](#)]
12. Malhotra, M.; Garg, N.; Chand, P.; Jakhete, A. Bio-based bioplastics: Current and future developments. In *Valorization of Biomass to Bioproducts*; Elsevier: Amsterdam, The Netherlands, 2023; pp. 475–504.
13. Ayu, R.; Khalina, A.; Harmaen, A.; Zaman, K.; Jawaid, M.; Lee, C. Effect of Modified Tapioca Starch on Mechanical, Thermal, and Morphological Properties of PBS Blends for Food Packaging. *Polymers* **2018**, *10*, 1187. [[CrossRef](#)]
14. Arnata, I.W.; Gunam, I.B.W.; Anggreni, A.A.M.D.; Wijaya, I.M.M.; Sartika, D. Utilization of solid tapioca waste for bioethanol production by co-fermentation of baker's and tapai yeast. *IOP Conf. Ser. Earth Environ. Sci.* **2021**, *724*, 012058. [[CrossRef](#)]
15. Situmorang, A.; Manik, Y. Initial sustainability assessment of tapioca starch production system in Lake Toba area. *IOP Conf. Ser. Mater. Sci. Eng.* **2018**, *337*, 012044. [[CrossRef](#)]
16. Luchese, C.L.; Rodrigues, R.B.; Tessaro, I.C. Cassava starch-processing residue utilization for packaging development. *Int. J. Biol. Macromol.* **2021**, *183*, 2238–2247. [[CrossRef](#)]
17. Matheus, J.R.V.; de Farias, P.M.; Satoriva, J.M.; de Andrade, C.J.; Fai, A.E.C. Cassava starch films for food packaging: Trends over the last decade and future research. *Int. J. Biol. Macromol.* **2023**, *225*, 658–672. [[CrossRef](#)]
18. Ogunjobi, J.K.; Adewale, A.I.; Adeyemi, S.A. Cellulose nanocrystals from Siam weed: Synthesis and physicochemical characterization. *Heliyon* **2023**, *9*, e13104. [[CrossRef](#)] [[PubMed](#)]
19. Eze, F.N.; Jayeoye, T.J. *Chromolaena odorata* (Siam weed): A natural reservoir of bioactive compounds with potent anti-fibrillogenic, antioxidative, and cytocompatible properties. *Biomed. Pharmacother.* **2021**, *141*, 111811. [[CrossRef](#)]
20. Mohamad, C.W.S.R.; Cheng, E.M.; Talib, N.A.A. Antibacterial Activity of Biodegradable Plastic from *Chromolaena odorata* (Pokok Kapal Terbang) Leaves. *J. Phys. Conf. Ser.* **2021**, *2071*, 012010. [[CrossRef](#)]
21. Dome, K.; Podgorbunskikh, E.; Bychkov, A.; Lomovsky, O. Changes in the Crystallinity Degree of Starch Having Different Types of Crystal Structure after Mechanical Pretreatment. *Polymers* **2020**, *12*, 641. [[CrossRef](#)] [[PubMed](#)]
22. Zobel, H.F. Starch Crystal Transformations and Their Industrial Importance. *Starch-Stärke* **1988**, *40*, 1–7. [[CrossRef](#)]
23. Chen, X.; Yao, W.; Gao, F.; Zheng, D.; Wang, Q.; Cao, J.; Tan, H.; Zhang, Y. Physicochemical Properties Comparative Analysis of Corn Starch and Cassava Starch, and Comparative Analysis as Adhesive. *J. Renew. Mater.* **2021**, *9*, 979–992. [[CrossRef](#)]
24. Zhu, X.; He, Q.; Hu, Y.; Huang, R.; Shao, N.; Gao, Y. A comparative study of structure, thermal degradation, and combustion behavior of starch from different plant sources. *J. Therm. Anal. Calorim.* **2018**, *132*, 927–935. [[CrossRef](#)]
25. Merhari, L.; Moliton, J.P.; Belorgeot, C. Fourier transform infrared study of ion irradiated nitrocellulose. *J. Appl. Phys.* **1990**, *68*, 4837–4845. [[CrossRef](#)]
26. Lomelí-Ramírez, M.G.; Barrios-Guzmán, A.J.; García-Enriquez, S.; Rivera-Prado, J.D.J.; Manríquez-González, R. Chemical and Mechanical Evaluation of Bio-composites Based on Thermoplastic Starch and Wood Particles Prepared by Thermal Compression. *BioResources* **2014**, *9*, 2960–2974. [[CrossRef](#)]
27. Swapna, M.S.; Sankararaman, S. Tuning the thermal diffusivity of the seed matter for enhanced biosynthesis: A thermal lens study. *Eur. Phys. J. Plus* **2020**, *135*, 224. [[CrossRef](#)]
28. Rashid, I.; Omari, M.H.A.; Leharne, S.A.; Chowdhry, B.Z.; Badwan, A. Starch gelatinization using sodium silicate: FTIR, DSC, XRPD, and NMR studies. *Starch-Stärke* **2012**, *64*, 713–728. [[CrossRef](#)]
29. Versino, F.; García, M.A. Starch films for agronomic applications: Comparative study of urea and glycerol as plasticizers. *Int. J. Environ. Agric. Biotechnol.* **2018**, *3*, 1854–1864. [[CrossRef](#)]
30. Monych, N.K.; Turner, R.J. Multiple Compounds Secreted by *Pseudomonas aeruginosa* Increase the Tolerance of *Staphylococcus aureus* to the Antimicrobial Metals Copper and Silver. *mSystems* **2020**, *5*, e00746-20. [[CrossRef](#)] [[PubMed](#)]
31. Pandur, E.; Tamási, K.; Pap, R.; Jánosa, G.; Sipos, K. Distinct Effects of *Escherichia coli*, *Pseudomonas aeruginosa* and *Staphylococcus aureus* Cell Wall Component-Induced Inflammation on the Iron Metabolism of THP-1 Cells. *Int. J. Mol. Sci.* **2021**, *22*, 1497. [[CrossRef](#)] [[PubMed](#)]
32. Abdallah, M.; Khelissa, O.; Ibrahim, A.; Benoliel, C.; Heliot, L.; Dhulster, P.; Chihib, N.-E. Impact of growth temperature and surface type on the resistance of *Pseudomonas aeruginosa* and *Staphylococcus aureus* biofilms to disinfectants. *Int. J. Food Microbiol.* **2015**, *214*, 38–47. [[CrossRef](#)]
33. Dayan, G.H.; Mohamed, N.; Scully, I.L.; Cooper, D.; Begier, E.; Eiden, J.; Jansen, K.U.; Gurtman, A.; Anderson, A.S. *Staphylococcus aureus*: The current state of disease, pathophysiology and strategies for prevention. *Expert Rev. Vaccines* **2016**, *15*, 1373–1392. [[CrossRef](#)]
34. Shineh, G.; Mobaraki, M.; Perves Bappy, M.J.; Mills, D.K. Biofilm Formation, and Related Impacts on Healthcare, Food Processing and Packaging, Industrial Manufacturing, Marine Industries, and Sanitation—A Review. *Appl. Microbiol.* **2023**, *3*, 629–665. [[CrossRef](#)]
35. Breijyeh, Z.; Jubeh, B.; Karaman, R. Resistance of Gram-Negative Bacteria to Current Antibacterial Agents and Approaches to Resolve It. *Molecules* **2020**, *25*, 1340. [[CrossRef](#)]
36. Huleihel, M.; Pavlov, V.; Erukhimovitch, V. The use of FTIR microscopy for the evaluation of anti-bacterial agents activity. *J. Photochem. Photobiol. B Biol.* **2009**, *96*, 17–23. [[CrossRef](#)] [[PubMed](#)]

37. Oliveira, R.N.; Mancini, M.C.; Oliveira, F.C.S.D.; Passos, T.M.; Quilty, B.; Thiré, R.M.D.S.M.; McGuinness, G.B. FTIR analysis and quantification of phenols and flavonoids of five commercially available plants extracts used in wound healing. *Matéria* **2016**, *21*, 767–779. [[CrossRef](#)]
38. Mueed, A.; Shibli, S.; Korma, S.A.; Madjirebaye, P.; Esatbeyoglu, T.; Deng, Z. Flaxseed Bioactive Compounds: Chemical Composition, Functional Properties, Food Applications and Health Benefits-Related Gut Microbes. *Foods* **2022**, *11*, 3307. [[CrossRef](#)] [[PubMed](#)]

Disclaimer/Publisher’s Note: The statements, opinions and data contained in all publications are solely those of the individual author(s) and contributor(s) and not of MDPI and/or the editor(s). MDPI and/or the editor(s) disclaim responsibility for any injury to people or property resulting from any ideas, methods, instructions or products referred to in the content.